Journal of Statistical Physics, Vol. 78, Nos. 1/2, 1995

Criteria for Local Equilibrium in a System with Transport of Heat and Mass

Bjørn Hafskjold[1] **and Signe Kjelstrup Ratkje**[1]

Received October 18, 1993

Nonequilibrium molecular dynamics is used to compute the coupled heat and mass transport in a binary isotope mixture of particles interacting with a Lennard-Jones/spline potential. Two different stationary states are studied, one with a fixed internal energy flux and zero mass flux, and the other with a fixed diffusive mass flux and zero temperature gradient. Computations are made for one overall temperature, $T = 2$, and three overall number densities, $n = 0.1$, 0.2, and 0.4. (All numerical values are given in reduced, Lennard-Jones units unless otherwise stated.) Temperature gradients are up to $\nabla T = 0.09$ and weight-fraction gradients up to $\nabla w_1 = 0.007$. The flux–force relationships are found to be linear over the entire range. All four transport coefficients (the L-matrix) are determined and the Onsager reciprocal relationship for the off-diagonal coefficients is verified. Four different criteria are used to analyze the concept of local equilibrium in the nonequilibrium system. The local temperature fluctuation is found to be $\delta T \approx 0.03T$ and of the same order as the maximum temperature difference across the control volume, except near the cold boundary. A comparison of the local potential energy, enthalpy, and pressure with the corresponding equilibrium values at the same temperature, density, and composition also verifies that local equilibrium is established, except near the boundaries of the system. The velocity contribution to the Boltzmann H-function agrees with its Maxwellian (equilibrium) value within 1%, except near the boundaries, where the deviation is up to 4%. Our results do not support the Eyring-type transport theory involving jumps across energy barriers; we find that its estimates for the heat and mass fluxes are wrong by at least one order of magnitude.

KEY WORDS: Nonequilibrium molecular dynamics; irreversible thermodynamics; Onsager reciprocal relations; local equilibrium.

[1] Department of Physical Chemistry, University of Trondheim, Norwegian Institute of Technology, N-7034 Trondheim, Norway.

0022-4715/95/0100-0463$07.50/0

1. INTRODUCTION

The assumption of local equilibrium is a basic and necessary assumption in linear irreversible thermodynamics. It enables us to apply the equations of equilibrium thermodynamics, such as the Gibbs equation, to *local* volume elements in a system. The entropy and other thermodynamic properties of the system can then be defined in terms of local, intensive state variables. The assumption leads to the concept of an *entropy production* in a system subject to irreversible processes. For a binary system with coupled heat and mass transport, which we shall consider in this paper, the entropy production per unit volume and unit time is

$$\sigma = -\mathbf{J}_q \cdot \frac{\nabla T}{T^2} - \mathbf{J}_1 \cdot \frac{\nabla_T(\mu_1 - \mu_2)}{T} \tag{1}$$

where $\mathbf{J}_q$ is the heat flux, $\mathbf{J}_1$ is the mass flux of component 1, T and ∇T are the temperature and the temperature gradient, respectively, and μ_k is the partial specific Gibbs energy of component k. The subscript T represents a gradient under isothermal conditions.

In the linear regime, i.e., for small fluxes and forces, the two independent fluxes are linear combinations of the forces,

$$\mathbf{J}_q = -L_{qq}\frac{\nabla T}{T^2} - L_{q1}\frac{1}{T}\nabla_T(\mu_1 - \mu_2) \tag{2a}$$

$$\mathbf{J}_1 = -L_{1q}\frac{\nabla T}{T^2} - L_{11}\frac{1}{T}\nabla_T(\mu_1 - \mu_2) \tag{2b}$$

Implicit in these equations is a choice of the barycentric frame of reference for the fluxes, in which $\mathbf{J}_1 = -\mathbf{J}_2$. Further details of the phenomenological basis for this paper are given in Section 2.

Onsager[1] assumed microscopic reversibility or local equilibrium in the derivation of his reciprocal relations (ORR), $L_{ij} = L_{ji}$ [cf. Eq. (2)]. The derivation was based on linear flux–force relationships. Kinetic theory indicates that the ORR are valid also beyond the linear regime,[2] while Olah states the opposite in his thermokinetic theory.[3,4] Tenenbaum *et al.*[5] found local equilibrium and a linear relationship between the heat flux and the temperature gradient in their nonequilibrium molecular dynamics (NEMD) simulations of heat conduction in a one-component Lennard-Jones system. They used temperature gradients as large as 1.8×10^{11} K m^{-1}. MacGowan and Evans[6] and Paolini and Ciccotti[7] also found local equilibrium for extremely large thermodynamic forces. These results raise several basic questions: How can we better quantify what we mean by local

equilibrium? Does it follow from observed linear flux–force relationships that local equilibrium exists? If the validity of the ORR goes beyond the linear regime, can they be more generally explained in terms of molecular properties?

In his discussion of the local equilibrium assumption, Kreuzer[8] considers volume elements that are small enough so that the thermodynamic properties vary little over each element, but large enough so that each element can be treated as a macroscopic thermodynamic subsystem. The meaning of *small* and *large* in this context is not precisely defined. A definition and its quantification must be based on statistical mechanics. For instance, "large enough" can be quantified by a lower limit on the fluctuations in the particle number, the temperature fluctuations, or a length scale comparable to the molecules' mean free path. If we consider a system subject to a temperature field, "small enough" can be quantified by comparing the temperature difference over a volume element with its local temperature fluctuations.

NEMD simulation is a useful tool for obtaining quantitative statistical information on a nonequilibrium many-body system. By analogy to equilibrium MD simulations, thermodynamic properties and transport properties are computed as averages over time in a stationary state. This implies that we assume local equilibrium. To what extent this assumption is valid can be examined in detail, which is a main topic of this paper. We show how NEMD can provide new information on nonequilibrium systems in a way that supplements experimental data. In particular, we shall discuss several criteria of local equilibrium and find out if they are consistent. Our aim is to contribute to the understanding of nonequilibrium systems.

Our model system is a supercritical binary mixture with heat and mass transport. A suitable size of the control volumes to be examined must first be chosen. The Chapman–Enskog solution of the Boltzmann equation shows that local equilibrium can be assumed in the dilute hard-sphere gas if the temperature variation over a mean free path is much smaller than the average temperature in the volume element.[9,10] For a liquid, the mean free path is of the same order as the molecular diameter, and the above argument cannot be applied. Following Kreuzer,[8] we consider a control volume of length l, which replaces the mean free path in the gas. The size of the control volume is determined from equilibrium fluctuation theory and the results of Tenenbaum *et al.*[5]; it is large enough so that the properties of the system can be precisely computed and their fluctuations are small. Exactly how small cannot be precisely stated, but Kreuzer[8] suggests that $\delta N/N \leqslant 10^{-2}$ for a liquid, where N is the number of particles in the control volume. Local equilibrium is maintained if $l\,|\nabla T|$, where ∇T is the temperature gradient, across a control volume is smaller than the

fluctuations in T. A combined criterion which would apply to our system is therefore[8]

$$l\,|\nabla T| \leqslant \delta T \tag{3a}$$

and

$$\delta T \ll T \tag{3b}$$

Tenenbaum *et al.*[5] discussed a local equilibrium criterion that essentially states that the local density in a nonequilibrium system must be equal (within statistical uncertainties) to the equilibrium value at the same temperature and pressure. This relates the concept of local equilibrium to the equation of state and use of thermodynamic properties as indicators of local equilibrium. Also in this case a suitable size of the control volume must be chosen. If it is too small, the statistics of the computed time averages is poor; if it is too large, the property of interest is not sufficiently uniform across the volume. Based on their calculations, they concluded that l is of the order of the intermolecular distance in a crystal lattice of the same substance. We apply this criterion to our system and compare it with the other criteria.

Haile[11] suggested, similarly to Orban and Bellemans,[12] that the velocity part of the Boltzmann H-function,

$$H = \int_{-\infty}^{\infty} f(\mathbf{v}) \ln f(\mathbf{v})\, d\mathbf{v} \tag{4}$$

can be used as an indicator of local equilibrium. If the velocity distribution function $f(\mathbf{v})$ is Maxwellian, H is given by its Maxwell value,

$$H_x = H_y = H_z = \frac{1}{3} H_{\mathrm{M}} = \frac{1}{2}\left[\ln\left(\frac{m}{2\pi k T}\right) - 1\right] \tag{5}$$

for a one-component system. In Eq. (5), H_x is the contribution to H_{M} in the x direction (and similarly for y and z), m is the molecular mass, and k is Boltzmann's constant. By comparing H to H_{M}, we obtain a measure of the deviation from the Maxwell–Boltzmann velocity distribution of the particles. This is also related to the thermodynamic properties; at equilibrium H_{M} equals $-S/k$ for an ideal gas, where S is the entropy. The size of the control volume in which the H-function is evaluated must be chosen according to the same criteria as those discussed above.

A final criterion that we consider is inspired by the Eyring rate theory for chemical reaction kinetics[13] and the overpotential theory for electric current across an interface, i.e., the Butler–Volmer equation.[14] The basic idea of the Butler–Volmer equation is that a net charge flux i, i.e., the

difference between the unidirectional charge fluxes i^+ and i^- in positive and negative directions, respectively, across the interface is

$$i = i^+ - i^- = i^0 \left[\exp\left(-\frac{\Delta\varphi}{2kT} \right) - \exp\left(+\frac{\Delta\varphi}{2kT} \right) \right] \tag{6}$$

where i^0 is the equilibrium value of i^+ and i^-, the so-called exchange current density, that is, the flux of electric charge in each direction at equilibrium. We shall refer to such an equilibrium value of a flux in one direction as a unidirectional flux. The value of i^0 is related to the activation energy of the current, and $\Delta\varphi$ is the driving force of the flux, in this case the overpotential. In general, this driving force is a potential difference over a distance comparable to a molecular diameter. The factor 1/2 in the exponential functions relates to the transport mechanism; if the resistance to the flux is caused by a well-defined energy barrier halfway between two stable positions, as in a lattice, the barrier height is $E_a + (-)\Delta\varphi/2$ in positive (negative) directions.[15] At equilibrium, $\Delta\varphi = 0$, and therefore $i = 0$. Linearization of Eq. (6) can be used as a criterion which puts a limit on both the flux and its conjugate force. The error made by linearizing $e^x - e^{-x}$ is 1% when $x = 0.31$ and 10% when $x = 0.66$. The following questions are therefore also interesting: Given that *linear* flux–force relations can be used as a measure of local equilibrium, what is the upper limit of i/i^0 for the linear range? How does this criterion of local equilibrium compare with the other criteria mentioned above?

The relation between the unidirectional fluxes at equilibrium and the L coefficients has been discussed for a one-dimensional Ising system by Hill,[16] in the thermokinetic theory by Olah,[3] and in general by Caplan and Essig.[17] Attempts have been made to use this relation in order to understand the lack of linear flux–force relations for ion transport in biological membranes.[17, 18]

For our heat and mass transport, the analogous force for the heat flux and the mass flux would be ΔT and $\Delta_T(\mu_1 - \mu_2)$, respectively, where Δ represents the difference across a control volume. A combined criterion for a 1% deviation from linearity would by analogy read

$$\frac{\mathbf{J}_1}{\mathbf{J}_1^0} < 0.3 \tag{7a}$$

and

$$\frac{\mathbf{J}_q}{\mathbf{J}_q^0} < 0.3 \tag{7b}$$

In Eq. (7), superscript 0 represents the equilibrium unidirectional fluxes, as in i^0 above.

In this work, we apply two different NEMD algorithms, one with emphasis on the heat flux and the other with emphasis on the mass flux in a binary liquid mixture. One of the algorithms, the "heat exchange" (HEX) algorithm, has been reported and discussed in detail by Ikeshoji and Hafskjold[19] and Hafskjold *et al.*[20] We apply the HEX algorithm to the different criteria for local equilibrium discussed above. A new "mass exchange" (MEX) algorithm will be used in combination with the HEX algorithm to compute all four transport coefficients in a binary mixture and test the Onsager reciprocal relationships (ORR). The algorithms are described in Section 3.

The calculations are described in Section 4, and the results are given in Section 5. A discussion of the different criteria [Eqs. (3)–(7)] is given in Section 6.

2. HEAT AND MASS FLUX IN A BINARY MIXTURE

We examine the local equilibrium criteria discussed in Section 1 by applying the HEX algorithm to an isotope mixture of Lennard-Jones/spline particles (see Section 4 for details of the model).

The thermal conductivity may be defined by solving (2b) for $\nabla_T(\mu_1 - \mu_2)$ and substituting this into (2a):

$$\lambda_{\mathbf{J}_1=0} = \frac{1}{T^2}\left(L_{qq} - \frac{L_{q1}L_{1q}}{L_{11}}\right) = -\left(\frac{\mathbf{J}_q}{\nabla T}\right)_{\mathbf{J}_1=0} \tag{8}$$

The thermal diffusion factor α_{12} is defined as

$$\alpha_{12} = -\left(\frac{\nabla \ln(w_1/w_2)}{\nabla \ln T}\right)_{\mathbf{J}_1=0} = -\frac{T}{w_1 w_2}\left(\frac{\nabla w_1}{\nabla T}\right)_{\mathbf{J}_1=0} = \frac{L_{1q}}{L_{11}}\frac{\partial \ln w_1}{\partial \mu_1} \tag{9}$$

where the last equation is derived by use of the Gibbs–Duhem equation for a binary mixture at uniform pressure,

$$\nabla_T(\mu_1, \mu_2) = \frac{1}{w_2}\frac{\partial \mu_1}{\partial w_1}\nabla w_1 \tag{10}$$

Here, w_k is the weight fraction of component k. The heat flux for nonzero mass flux may be written as

$$\mathbf{J}_q = -\lambda_{\mathbf{J}_1=0}\nabla T + q^*\mathbf{J}_1 \tag{11}$$

where q^* is the heat of transfer,

$$q^* = \frac{L_{q1}}{L_{11}} = \frac{\mathbf{J}_q + \lambda_{\mathbf{J}_1=0} \nabla T}{\mathbf{J}_1} \tag{12a}$$

or, alternatively,

$$q^* = \left(\frac{\mathbf{J}_q}{\mathbf{J}_1}\right)_{\nabla T=0} \tag{12b}$$

The ratio L_{q1}/L_{1q} is given by

$$\frac{L_{q1}}{L_{1q}} = \frac{q^*}{\alpha_{12}} \frac{\partial \ln w_1}{\partial \mu_1} \tag{13}$$

If the ORR is valid, the ratio is unity. The mass flux may be expressed as

$$\mathbf{J}_1 = -\rho w_1 D(w_2 \alpha_{12} \nabla T + \nabla \ln w_1) \tag{14}$$

where ρ is the mass density and D is the diffusion coefficient,

$$D = \frac{L_{11}}{\rho w_2 T} \frac{\partial \mu_1}{\partial w_1} \tag{15}$$

If the thermal conductivity, thermal diffusion factor, heat of transfer, and diffusion coefficient can be computed by NEMD, Eqs. (8), (9), (12), and (15) may be solved for the L coefficients.

For an ideal mixture, such as a mixture of isotopes, the derivative of the partial specific Gibbs energy at zero pressure gradient simplifies to

$$\frac{\partial \mu_1}{\partial w_1} = \frac{k_B T}{w_1(m_1 w_2 + m_2 w_1)} \tag{16}$$

The thermal diffusion factor is then

$$\alpha_{12} = \frac{L_{1q}}{L_{11}} \frac{(m_1 w_2 + m_2 w_1)}{k_B T} \tag{17}$$

and the diffusion coefficient becomes

$$D = L_{11} \frac{k_B}{\rho w_1 w_2 (m_1 w_2 + m_2 w_1)} \tag{18}$$

The heat flux for a binary mixture is related to the internal energy flux by

$$\mathbf{J}_q = \mathbf{J}_U - (h_1 - h_2)\mathbf{J}_1 \tag{19}$$

where h_k is the partial specific enthalpy. For an ideal mixture, h_k is independent of the composition and equal to the specific enthalpy of pure component k. In this paper, we consider an isotope mixture with molecular masses m_k. We then have $h_k = m_n h_n / m_k$ and therefore

$$\mathbf{J}_q = \mathbf{J}_U - h_2 \left(\frac{m_2}{m_1} - 1 \right) \mathbf{J}_1 \tag{20}$$

At a stationary state where $\mathbf{J}_k = 0$, we have $\mathbf{J}_U = \mathbf{J}_q$. Whereas $\mathbf{J}_U$ in general depends on a reference state for the potential energy or μ_k, $\mathbf{J}_q$ does not. Moreover, in the absence of viscous forces, $\mathbf{J}_q$ is also independent of the frame of reference.[21]

3. THE NEMD ALGORITHMS

The internal energy flux $\mathbf{J}_U$ may be computed by NEMD according to[22]

$$\mathbf{J}_U = \frac{1}{V} \sum_{i \in \mathrm{CV}} \left([\tfrac{1}{2} m_i (\mathbf{v}_i - \mathbf{v})^2 + \phi_i] (\mathbf{v}_i - \mathbf{v}) - \tfrac{1}{2} \sum_{\substack{j=1 \\ j \neq i}}^{N} [(\mathbf{v}_i - \mathbf{v}) \cdot \mathbf{F}_{ij}] \mathbf{r}_{ij} \right) \tag{21}$$

where V is the size of the control volume (CV), m_i and $\mathbf{v}_i$ are the mass and velocity, respectively, of particle i, $\mathbf{v}$ is the barycentric velocity of the system, ϕ_i is the potential energy of particle i in the field of all the other particles, $\mathbf{F}_{ij}$ is the force acting on i due to j, and $\mathbf{r}_{ij}$ is the vector from the position of i to the position of j. This is a local, instantaneous version of the macroscopic internal energy flux.

Equation (21) suggests that the internal energy flux may be interpreted in terms of three contributions. The first and second terms are the kinetic and potential energy, respectively, carried by a moving particle. The third term is the intermolecular energy transfer due to motion of a particle in the field of the other particles.

The mass flux of component k is

$$\mathbf{J}_k = \frac{1}{V} \sum_{i \in \mathrm{CV} \cup k} m_i (\mathbf{v}_i - \mathbf{v}) \tag{22}$$

where the summation is performed over particles i of type k in the CV. The temperature gradient is given in NEMD by computations of the local temperature according to

$$\tfrac{3}{2}NkT = \tfrac{1}{2}\sum_{i \in \mathrm{CV}}^{N} m_i(\mathbf{v}_i - \mathbf{v})^2 \tag{23}$$

where N is the number of particles in the control volume. Strictly speaking, $3N$ represents the number of degrees of freedom. In each control volume, which is an open system, the number of degrees of freedom equals $3N$. With the fluxes, the local temperatures, and the local compositions, we can examine the flux–force relationships.

Our approach to investigate the ORR is to make two different boundary-driven NEMD simulations, one with the "heat exchange" (HEX) algorithm in which $\mathbf{J}_U$ is fixed by the boundary conditions and $\mathbf{J}_1$ is determined by the system, and another with the "mass exchange" (MEX) algorithm in which $\mathbf{J}_1$ is fixed by the boundary conditions and $\mathbf{J}_U$ is determined by the system. In both cases, a stationary state is reached, and the system's properties can be computed. For the heat exchange algorithm, $\mathbf{J}_1$ equals zero in the stationary state.

The HEX algorithm was described in previous papers[19, 20] and will only be briefly mentioned here. The MEX algorithm is not described elsewhere, and will be explained in detail necessary for the later discussion of the results. A full description of the MEX algorithm will be made in a

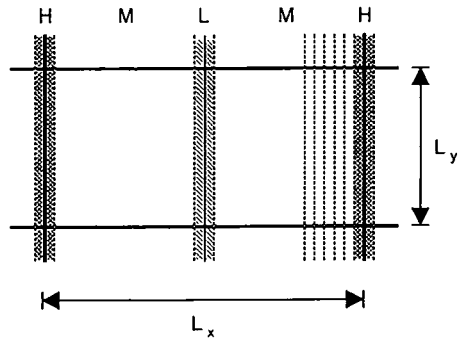

Fig. 1. Layout of the MD cell showing the periodic boundary conditions. The different regions are: H, where energy is supplied in the HEX algorithm and particles swap from light to heavy in the MEX algorithm; L, where energy is withdrawn in the HEX algorithm and particles swap from heavy to light in the MEX algorithm; and M, where the transport is analyzed. The cell is divided into 32 layers perpendicular to the x axis, some of which are shown here.

forthcoming paper. In both cases we used a MD cell which was divided into 32 layers perpendicular to the x axis as shown in Fig. 1. The layers form three regions, marked H, M, and L. Region H has high temperature in case of the HEX algorithm and a surplus of heavy particles in the MEX algorithm. Region L has low temperature in the HEX algorithm and a surplus of light particles in the MEX algorithm. The middle regions were used for computations of the local density, temperature, composition, mass fluxes, energy flux, energy, and other quantities of interest.

3.1. The HEX Algorithm

The energy flux through the system was generated by adding a certain amount of kinetic energy to the system in region H and taking out the same amount of kinetic energy in region L at each time step. As a consequence, the system developed an internal energy flux and a temperature gradient. The barycentric velocity of the total system is zero if the numerical algorithm conserves the initial zero momentum.

The velocities of all the particles in region H (L) were scaled according to the amount of added (withdrawn) energy, $(-)\,\Delta U$, and shifted in order to conserve a zero momentum of the total system. If the velocity of particle i before energy addition was $\mathbf{v}_i'$, then the velocity after energy addition is

$$\mathbf{v}_i = (1+\alpha)\mathbf{v}_i' + \boldsymbol{\beta} \tag{24}$$

where

$$\boldsymbol{\beta} = -\frac{\alpha \sum m_i \mathbf{v}_i'}{\sum m_i} \tag{25}$$

The summation is done over all the particles in region H (L). A specified value of ΔU leads to a quadratic equation in α:

$$(-)\,\Delta U = \tfrac{1}{2}\sum m_i \{[(1+\alpha)\mathbf{v}_i' + \boldsymbol{\beta}]^2 - \mathbf{v}_i'^2\} \tag{26}$$

At stationary state, the x component of the internal energy flux must equal half the rate at which energy is added and removed in the hot and cold regions, respectively,

$$\mathbf{J}_U = \left\{\frac{\text{sign}(x)\,\Delta U}{2\,\delta t\, L_y L_z}, 0, 0\right\} \tag{27}$$

where sign(x) is in + (−) in the left (right) half of the MD cell, δt is the time step, and L_y and L_z are the cell dimensions in y and z directions, respectively. The internal energy fluxes computed from Eqs. (21) and (27) were compared and used as a test of internal consistency of the algorithm.

3.2. The MEX Algorithm

The mass flux through the system was generated by changing a particle from species 2 (light) to species 1 (heavy) in region H and simultaneously from species 1 to 2 in region L at regular intervals, according to the specified mass flux. This is essentially the same technique as the "particle swapping" algorithm discussed by Sindzingre *et al.*[23] As a consequence, the system developed a mass flux and a concentration gradient. The velocity of the swapped particle was first scaled so that the particle maintained its kinetic energy. This was done in order to avoid a large, local source (sink) of kinetic energy when a light (heavy) particle changed type. The velocities of all the particles in regions H and L were then scaled and shifted in order to conserve the energy and the momentum of each region and the total system. If the velocity and mass of the swapped particle s before swapping were $\mathbf{v}'_s$ and m'_s, respectively, then the velocity after swapping is

$$\mathbf{v}_s = (1+\alpha)\left(\frac{m'_s}{m_s}\right)^{1/2}\mathbf{v}'_s + \boldsymbol{\beta} \tag{28}$$

where m_s is the mass of s after swapping. The velocities of all the other particles in each region after swapping is

$$\mathbf{v}_i = (1+\alpha)\mathbf{v}'_i + \boldsymbol{\beta}; \qquad i \neq s \tag{29}$$

The velocity shift in Eqs. (28) and (29) is given by

$$\boldsymbol{\beta} = -\frac{\alpha(\mathbf{P}+\Delta\mathbf{P})+\Delta\mathbf{P}}{M} \tag{30}$$

where

$$M = \sum m'_i \tag{31}$$

$$\mathbf{P} = \sum m'_i\mathbf{v}'_i \tag{32}$$

and

$$\Delta\mathbf{P} = [(m_s m'_s)^{1/2} - m'_s]\mathbf{v}'_s \tag{33}$$

The summation is done over all the particles (including s) in region H (L). The energy conservation in each region leads to a quadratic equation in α:

$$\alpha(2+\alpha)E+(1+\alpha)\boldsymbol{\beta}\cdot(\mathbf{P}+\Delta\mathbf{P})+\tfrac{1}{2}\beta^2 M+\Delta\phi_s=0 \tag{34}$$

where

$$E=\tfrac{1}{2}\sum m_i'\mathbf{v}_i'^2 \tag{35}$$

and $\Delta\phi_s$ is the change in potential energy of s due to the swapping. In the present isotope mixture, $\Delta\phi_s$ is identically zero.

Since a mass flux is induced by the MEX algorithm, we must establish the relationship between the barycentric frame of reference used in the phenomenological description, Eqs. (8)–(20) and the frame of reference used in the NEMD simulations. The coordinates and velocities of the particles are given in the "laboratory" fixed frame of reference, relative to the MD cell, as indicated by the superscript $\square$. In this frame of reference, the sum of the diffusive and convective mass fluxes of component k is $\mathbf{J}_k^{\square}$,

$$\mathbf{J}_k^{\square}=\rho_k\mathbf{v}_k^{\square} \tag{36}$$

where ρ_k is the mass density of component k. At the stationary state, the flux in the middle region must equal the source and sink terms in region H and L,

$$\mathbf{J}_k^{\square}=\left\{\frac{\operatorname{sign}_k m_k}{2\,\Delta t\,L_y L_z},0,0\right\} \tag{37}$$

Here sign_k is the sign $+$ $(-)$ for species 1 in the left (right) half of the MD cell and $-$ $(+)$ for species 2 in the left (right) half cell, subscript k represents species k, and Δt is the time between two particle swaps. The ratio between the x components of $\mathbf{J}_1^{\square}$ and $\mathbf{J}_2^{\square}$ is

$$\frac{J_{1,x}^{\square}}{J_{2,x}^{\square}}=-\frac{m_1}{m_2} \tag{38}$$

which leads to

$$\rho v_x=J_{1,x}^{\square}+J_{2,x}^{\square}=\left(1-\frac{m_2}{m_1}\right)J_{1,x}^{\square} \tag{39}$$

where ρ is the total mass density and v_x is the x component of $\mathbf{v}$. The y and z components of $\mathbf{v}$ are zero.

The mass flux of component k in the barycentric frame of reference is

$$\mathbf{J}_k = \rho_k(\mathbf{v}_k^{\square} - \mathbf{v}^{\square}) \tag{40}$$

Combination of Eqs. (36), (39), and (40) gives

$$\mathbf{J}_1 = \frac{w_1 m_2 + w_2 m_1}{m_1} \mathbf{J}_1^{\square} = m_2 \frac{n(x)}{\rho(x)} \mathbf{J}_1^{\square} \tag{41}$$

where w_k is the weight fraction of species k, and $n(x)$ and $\rho(x)$ are the local number density and mass density, respectively.

The *total* energy flux in the laboratory-fixed frame of reference $\mathbf{J}_E^{\square}$ is

$$\mathbf{J}_E^{\square} = \frac{1}{V} \sum_{i \in \mathrm{CV}} \left((\tfrac{1}{2} m_i \mathbf{v}_i^2 + \phi_i) \mathbf{v}_i - \tfrac{1}{2} \sum_{\substack{j=1 \\ j \neq i}}^{N} \mathbf{v}_i \cdot \mathbf{F}_{ij} \mathbf{r}_{ij} \right) \tag{42}$$

Like the internal energy flux in the HEX algorithm, the total energy flux is given by the heat exchange with the surroundings, Eq. (27), at the stationary state. If there is no heat exchange, $\mathbf{J}_E^{\square}$ is zero. This feature of the average *total* energy flux is useful for computation of the *internal* energy flux from Eq. (43),

$$\mathbf{J}_U = \mathbf{J}_E^{\square} - \frac{1}{V} \sum_{i \in \mathrm{CV}} \left[(\tfrac{1}{2} m_i \mathbf{v}^2 + \phi_i) \mathbf{v} - \tfrac{1}{2} \sum_{\substack{j=1 \\ j \neq i}}^{N} \mathbf{v} \cdot \mathbf{F}_{ij} \mathbf{r}_{ij} + \tfrac{1}{2} m_i (v_i^2 \mathbf{v} - v^2 \mathbf{v}_i) + m_i v_i \cdot v (\mathbf{v}_i - \mathbf{v}) \right] \tag{43}$$

Equation (43) gives a more precise average for $\mathbf{J}_U$ than does Eq. (21).

4. SYSTEM AND COMPUTATIONS

4.1. Pair Potential and Reduced Variables

A binary isotope mixture was modeled with the Lennard-Jones/spline potential[24]:

$$u_{ij}(r) = \begin{cases} 4\varepsilon_{ij} \left[\left(\dfrac{\sigma_{ij}}{r} \right)^{12} - \left(\dfrac{\sigma_{ij}}{r} \right)^{6} \right] & \text{for } r \leqslant r_s \\ a_{ij}(r - r_c)^2 + b_{ij}(r - r_c)^3 & \text{for } r_s \leqslant r \leqslant r_c \\ 0 & \text{for } r \geqslant r_c \end{cases} \tag{44}$$

where

$$r_s = \left(\frac{26}{7}\right)^{1/6} \sigma_{ij} \approx 1.244\sigma_{ij}$$

$$r_c = \frac{67}{48} r_s \approx 1.737\sigma_{ij}$$

$$a_{ij} = -\frac{24192}{3211} \frac{\varepsilon_{ij}}{r_s^2}$$

and

$$b_{ij} = -\frac{387072}{61009} \frac{\varepsilon_{ij}}{r_s^3}$$

The parameters σ_{ij} and ε_{ij} represent the molecular diameters and intermolecular potential depths, respectively.

Table I. Transport Coefficients for the Lennard-Jones/Spline System[a]

Run no.	n^*	J_q^*	$J_1^* \times 10^3$	λ^*	α_{12}	D_{12}^*	q^{**}
1[b]	0.1	0.1	0	1.149 ± 0.002	0.39 ± 0.02	N/A	N/A
2[c]	0.1		0.3636	N/A	N/A	4.7 ± 0.4	0.9
3[d]	0.1		0.5455	N/A	N/A	4.9 ± 0.3	4.9 ± 0.5
4[c]	0.1		0.9091	N/A	N/A	5.0 ± 0.2	5.4 ± 0.9
5[e]	0.1		1.8182	N/A	N/A	4.93 ± 0.03	3.7 ± 0.4
6[c,f]	0.153	0.1	0	1.139 ± 0.003	0.35 ± 0.03	N/A	N/A
7[e,f]	0.153		1.8182	N/A	N/A	2.38 ± 0.01	2.6 ± 0.2
8[b]	0.2	0.2	0	1.628 ± 0.001	0.60 ± 0.03	N/A	N/A
9[c]	0.2		0.3636	N/A	N/A	2.4 ± 0.3	10 ± 1
10[c]	0.2		0.7273	N/A	N/A	2.8 ± 0.2	2.8 ± 0.2
11[g]	0.2		1.8182	N/A	N/A	2.62 ± 0.03	5.7 ± 0.6
12[c]	0.2		2.7273	N/A	N/A	2.60 ± 0.05	6.6 ± 0.1
13[b]	0.4	0.3	0	2.639 ± 0.006	1.19 ± 0.02	N/A	N/A
14[e]	0.4		1.8182	N/A	N/A	1.14 ± 0.02	13.8 ± 0.7
15[c]	0.4		3.6364	N/A	N/A	1.15 ± 0.02	11.7 ± 0.1

[a] All results are given in reduced Lennard-Jones units. The uncertainties are given as one standard deviation. N/A, not available.
[b] Average of three runs of 2 million time steps each.
[c] One run of 4 million time steps.
[d] One run of 8 million time steps.
[e] Average of six runs of 2 million time steps each.
[f] Overall temperature $T^* = 1.35$.
[g] Average of seven runs of 2 million time steps each.

All the results are given in "Lennard-Jones units" (denoted by an asterisk) except when otherwise stated.

The thermodynamic states used in this work are listed in Table I. Unless stated otherwise, the overall system temperature was $T^* = 2.0$. The states are supercritical for the isotope mixture.

The mixture was equimolar, consisting in most cases of 512 particles (256 of each type) in a box of volume $V = L_x L_y L_z$ with periodic boundary conditions. The box was noncubic, with $L_y/L_x = L_z/L_x = 0.5$. The system was divided into N_L layers of equal thickness and perpendicular to the x axis in order to enable computations of the local density, temperature, composition, energy flux, energy, and other quantities of interest. For most runs, N_L was equal to 32. The thickness of each layer is (in Lennard-Jones units)

$$l_x^* = \frac{1}{N_L}\left(\frac{4N}{n^*}\right)^{1/3} \tag{45}$$

4.2. The Computations

All computations were made on an IBM RS6000/350 workstation. The HEX and the MEX codes ran at 44 and 27 time steps per CPU second, respectively, for 512 particles. Both algorithms conserve total energy and momentum to the extent documented by Hafskjold *et al.*[20]

Each run with the HEX code included 2,000,000 time steps of length $\delta t^* = 0.002$, starting from a randomized configuration or a previous run. The first 400,000 time steps of each run were discarded to avoid transient effects. A temperature drift was usually observed in the beginning of each run. If the drift exceeded a certain limit during the first 20,000 time steps, or if the initial temperature was not as specified, the velocities were scaled (subject to conservation of total momentum) to the set temperature. The internal energy flux was computed at each 20th time step, and subaverages were taken over 1000 instantaneous flux calculations, i.e., at 20,000-time step intervals, and dumped to file for later analysis. Several parallel runs were made for each thermodynamic state, as indicated in Table I. The statistical analysis was made considering the parallels to be independent.

In a series of test runs with the MEX algorithm we set $\mathbf{J}_E^{\square} = 0$ (no energy input or output). A small temperature gradient was established due to the Dufour effect. The heat flux was computed from Eqs. (20) and (21), assuming an ideal mixture (which is correct for an isotope mixture). Parallel runs did not give a satisfactory reproducibility of the heat of transfer as computed from Eq. (12a). A slight modification of the algorithm,

where we thermostatted regions H and L by a simple velocity scaling at each time step, enabled us to compute the heat of transfer from Eq. (12b). This gave a better reproducibility, and the final runs were made with six or more parallels of 2,000,000 time steps each. The runs were otherwise made the same way as with the HEX algorithm.

5. RESULTS

The HEX algorithm develops a stationary state with temperature and composition profiles as shown in Fig. 2a for $n^* = 0.1$. The heat flux is preset and the mass flux is zero. Similarly, the MEX algorithm gives the profiles shown in Fig. 2b. In this case, the mass flux is preset, and the heat flux is given by the requirements of the thermostats. On this basis, the transport coefficients λ^*, α_{12}, D^*, and q^* were computed at $T^* = 2.0$. Pairs

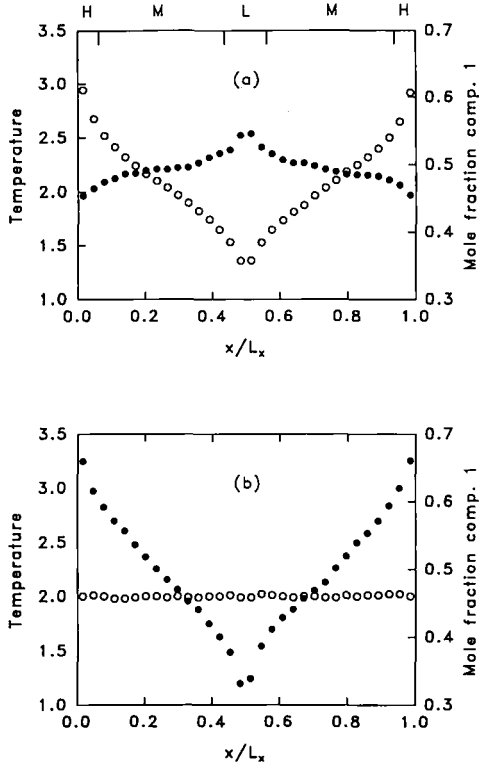

Fig. 2. The temperature (open circles) and mole fraction of component 1 (heavy component, solid circles) as function of x/L_x at the overall conditions $n^* = 0.1$ and $T^* = 2.0$. Data from the (a) HEX and (b) MEX algorithms. The locations of regions H, M, and L are also shown.

of data from the two symmetric half-cells were pooled and second-order polynomials were fitted to determine the gradients. The resulting data are given in Table I. The density dependence of the transport coefficients is not the topic of this paper, and will be discussed elsewhere.

The *local* temperature, density, and composition are not restricted to the preset values for the total cell. A layer in the center of the middle region will, however, be close to the overall conditions. Consequently, the conditions for the reported local properties will deviate only slightly from the overall conditions as shown in Table I.

The temperature profile in Fig. 2a is almost linear in the middle region, which means that the thermal conductivity is constant. (The heat flux is constant.)

The transport coefficients are shown as function of number density for equimolar mixtures at $T^* = 2$ in Fig. 3. The data on α_{12} supplement earlier data by Kincaid *et al.*[25] and Kincaid and Hafskjold[26] for the same system, but obtained with different boundary conditions (the fuzzy wall algorithm).

The heat flux is shown as function of the temperature gradient at zero mass flux in Fig. 4a, and the mass flux as function of the concentration gradient, $\rho \nabla w_1$, at zero temperature gradient in Fig. 4b. Both graphs show linear flux–force relationships.

Equations (8), (9), (12), and (15) were solved for the L coefficients, given the values of the transport coefficients and the fact that the mixture is ideal, Eq. (16). The results are given in Table II for $T^* = 2.0$. The main features of the L coefficients are: (1) L_{11} is constant over the studied

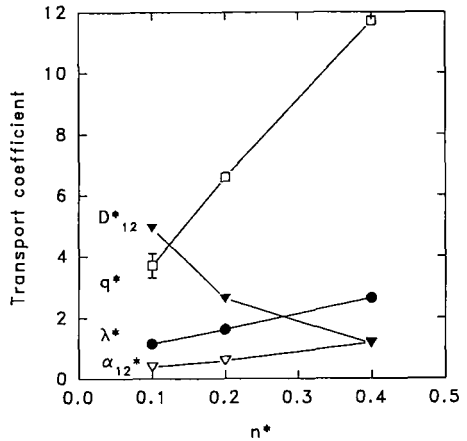

Fig. 3. The thermal conductivity (λ^*), mutual diffusion coefficient (D_{12}^*), thermal diffusion factor (α_{12}^*), and heat of transfer (q^*) as function of reduced number density for $T^* = 2.0$.

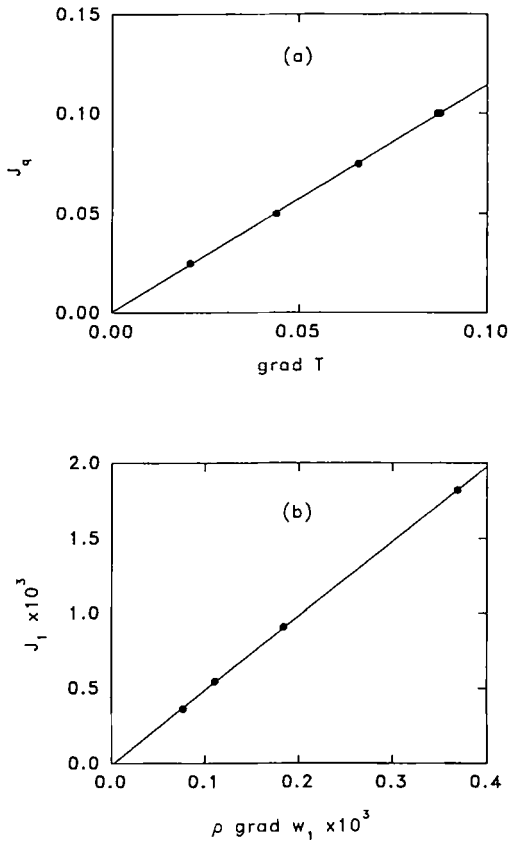

Fig. 4. (a) Heat flux as function of the temperature gradient and (b) mass flux as function of the concentration gradient, at $n^* = 0.1$ and $T^* = 2.0$. The data show linear flux–force relationships over the entire range we have studied. Both fluxes and forces are given in reduced Lennard-Jones units.

density range, (2) L_{q1}, L_{1q}, and L_{qq} are proportional to the density, (3) L_{1q} equals L_{q1} within the combined statistical uncertainties, and (4) L_{qq} contributes more than 94% to λ^* [cf. Eq. (8)], and the contribution decreases with increasing density.

Three different values of the size of the control volume were examined, $N_L = 32$, 16, and 8. The fluctuation in the particle number of a selected layer in the middle region is shown as function of time in Fig. 5 for $n^* = 0.1$ and $N_L = 32$. Time averages are given in Table IIIa for a more extensive set of states. Runs with 100,000 time steps were used in all cases. Calculations were made for each overall density (0.1, 0.2, and 0.4) in the hottest layer,

Table II. L Coefficients for the Lennard-Jones/Spline System[a]

n^*	ρ^*	$L_{11}^* \times 10^3$	L_{q1}^*	L_{1q}^*	L_{qq}^*	L_{q1}^*/L_{1q}^*
0.1	0.055	4.08 ± 0.03	0.015 ± 0.002	0.017 ± 0.001	4.66 ± 0.01	0.9 ± 0.1
0.153	0.084	3.01 ± 0.01	0.008 ± 0.001	0.008 ± 0.001	2.10 ± 0.01	1.0 ± 0.1
0.2	0.11	4.34 ± 0.05	0.025 ± 0.003	0.029 ± 0.001	6.68 ± 0.02	0.9 ± 0.1
0.4	0.22	3.78 ± 0.07	0.052 ± 0.003	0.049 ± 0.001	11.23 ± 0.05	1.06 ± 0.06

[a] All results are given in reduced Lennard-Jones units. The uncertainties are given as one standard deviation. The temperature is $T^* = 2.0$, except at $n^* = 0.153$, where $T^* = 1.35$.

a layer in the middle region corresponding to the average system temperature, and the coldest layer. The fluctuation in a quantity, e.g., the particle number, is given by

$$\delta N = \left[\frac{\sum_{i=1}^{n} (N_i - \langle N \rangle)^2}{n-1} \right]^{1/2} \tag{46}$$

where n is the number of instantaneous values and $\langle \cdots \rangle$ represents the time average.

The temperatures in three selected layers at $n^* = 0.1$ are shown as function of time in Fig. 6 and time averages are given for several states in Table IIIa. The local temperature fluctuations are also shown as error bars together with the temperature profile for half the cell in Fig. 7.

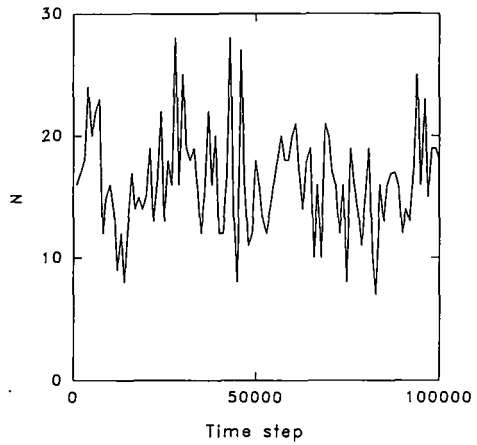

Fig. 5. Instantaneous particle numbers in a central layer in region M at $n^* = 0.1$ and $T^* = 2.0$ as a function of time.

Table III. Averages and Fluctuations in Local Particle Number and Local Temperature

n^*	l_x^*	N	δN	$\delta N/N$	T^*	δT^*	$\delta T/T$
a. 32 layers							
0.07	0.85	11.4	3.2	0.28	2.95	0.11	0.04
		(77.1)	(8.4)	(0.11)			
0.10	0.85	16.3	4.3	0.26	1.90	0.06	0.03
		(122.2)	(11.9)	(0.10)			
0.15	0.85	24.9	4.3	0.17	1.33	0.04	0.03
		(255.1)	(15.7)	(0.06)			
0.13	0.68	11.2	2.3	0.21	2.99	0.09	0.03
0.20	0.68	16.5	3.6	0.22	1.96	0.05	0.03
0.31	0.68	24.4	4.6	0.19	1.38	0.03	0.02
0.32	0.54	13.0	3.3	0.25	2.61	0.06	0.02
0.41	0.54	17.0	3.0	0.18	1.93	0.04	0.02
0.50	0.54	19.6	3.3	0.17	1.52	0.03	0.02
b. 16 layers							
0.1	1.71	29.5	4.7	0.16			
0.2	1.36	40.4	5.6	0.14			
0.4	1.08	30.7	3.9	0.13			
c. 8 layers							
0.1	3.42	68.6	7.5	0.11			
0.2	2.71	65.5	7.5	0.11			
0.4	2.16	67.1	5.7	0.08			

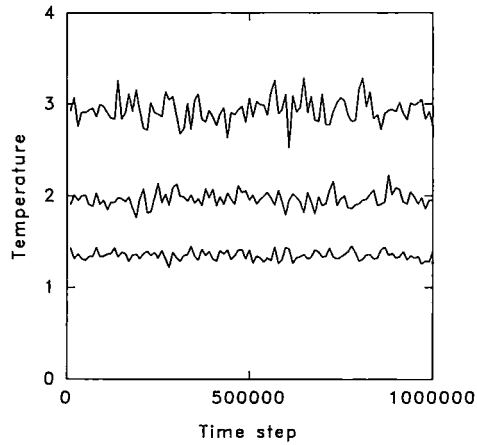

Fig. 6. Instantaneous temperatures in the hottest layer (upper curve), a central layer in region M (middle curve), and the coldest layer (lower curve) at $n^* = 0.1$ and $T^* = 2.0$ as a function of time.

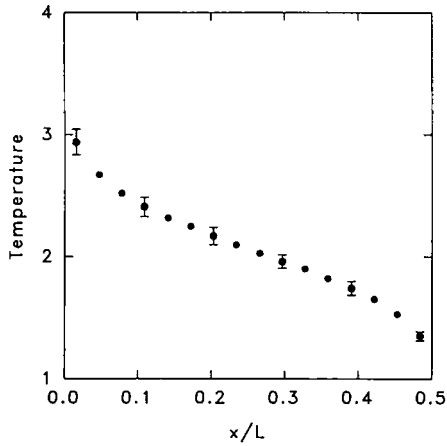

Fig. 7. The temperature profile across half the cell at $n^* = 0.1$ and $T^* = 2.0$. Also shown as error bars are the temperature fluctuations in some selected layers.

Each control volume is in the stationary, nonequilibrium state characterized by a density, temperature, and composition. For five of the layers, we performed equilibrium MD simulations at the local conditions in order to compare with the nonequilibrium properties. The results for pressure, potential energy, and enthalpy are shown in Fig. 8. For the layers in the middle region, there is excellent agreement between the equilibrium MD

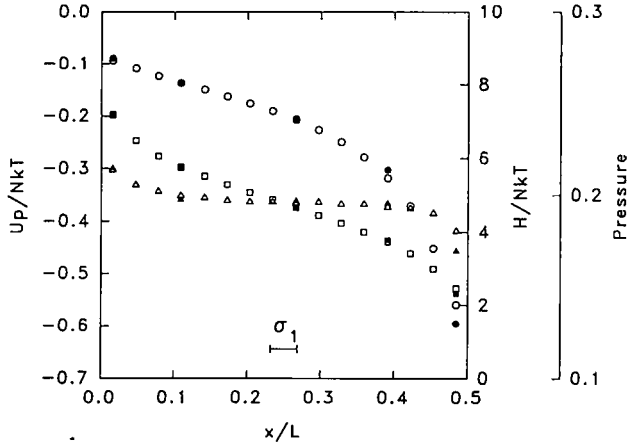

Fig. 8. Local values of the potential energy (squares), enthalpy (circles), and pressure (triangles) computed in a nonequilibrium run at $n^* = 0.1$ and $T^* = 2.0$ (open symbols) compared with the equilibrium values at the same conditions (solid symbols). The length scale of one molecular diameter is also shown.

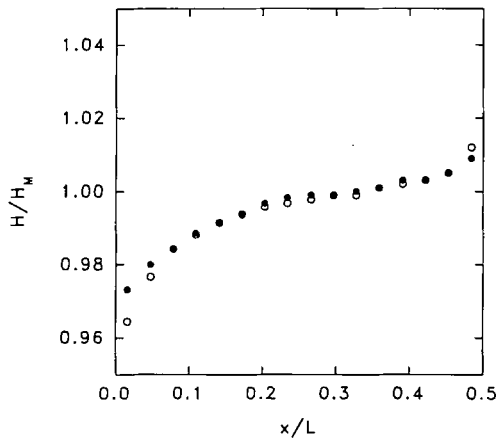

Fig. 9. The ratio between the Boltzmann H-function computed by NEMD and the Maxwellian value at the same temperature. The solid and the open symbols represent component 1 (heavy) and 2 (light), respectively.

and NEMD results. The clear disagreement in region L (the cold region) is discussed in Section 6.3.

The Boltzmann H-function was calculated for each control volume and compared to the results H_M with a Maxwell–Boltzmann distribution, Eq. (5). The results for the x component at $n^* = 0.1$ and $T^* = 2$ are given in Fig. 9. The relaxation toward the stationary state distribution as

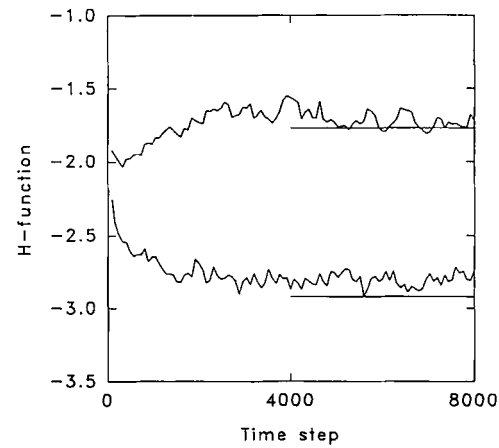

Fig. 10. Relaxation of the Boltzmann H-function, starting from a rectangular velocity distribution function, for the heavy (upper curve) and light (lower curve) components. The corresponding Maxwellian values at the stationary state are shown as horizontal lines.

indicated by the H-function was determined for each component, starting from a rectangular velocity distribution. This is illustrated in Fig. 10 for a layer in the middle region.

The internal energy flux, which is preset in the HEX algorithm, was also computed from Eq. (21). The local time averages of the flux were in good agreement with the preset value, as shown by Hafskjold *et al.*[20] Equation (21) gives the instantaneous values and it allows us to determine the equilibrium exchange flux $\mathbf{J}_q^0$ and the fluctuation in the heat flux δJ_q. The value of $J_{q,x}^0$ (the unidirectional heat flux in positive or negative x direction) was determined from an equilibrium run at $n^* = 0.1$ and $T^* = 2.0$–0.525 (in Lennard-Jones units), whereas the largest heat flux we used in the nonequilibrium runs was 0.1. This gives $\mathbf{J}_q/\mathbf{J}_q^0 \approx 0.2$ in the "worst" case. We found that the fluctuation δJ_q was of the same order as $J_{q,x}^0$. The corresponding value for $l\,|\nabla T|/2T$ is 0.02.

The value of $J_{1,x}^0$ was determined from the same equilibrium run as above to 0.00022 (in Lennard-Jones units), whereas the largest mass flux we used was 0.0018. This gives $\mathbf{J}_1/\mathbf{J}_1^0 \approx 8$ in the "worst" case. The corresponding value for $l\,|\nabla_T(\mu_1 - \mu_2)|/2kT$ is 0.2.

6. DISCUSSION

If the system would show lack of local equilibrium, nonlinear flux–force relationships, or violation of the ORR, we expected that this would occur at the lowest density, where the molecular mean free path is longest. Most of this discussion is therefore based on the data at $n^* = 0.1$.

6.1. Size of the Control Volume and Particle Number Fluctuations

Tenenbaum *et al.*[5] found that the size of the control volume could be chosen roughly equal to the molecular diameter, that is $l_x^* = 1$, in order to achieve acceptable statistics and local equilibrium. If $n^* = 0.1$, an l_x^* value of unity corresponds to $N_L = 27$ with 512 particles in the total system. The experience of Tenenbaum *et al.* may be compared to Kreuzer's suggestion of $\delta N/N \leqslant 10^{-2}$ with the data in Table III.

The two criteria for control volume size are not independent. The local particle number N is proportional to l^* and $\delta N/N$ is of order $1/N^{1/2}$. The fluctuation is related to the system's compressibility by

$$\frac{\delta N}{N} = \left(\frac{kT\kappa_T}{V}\right)^{1/2} \tag{47}$$

where κ_T is the isothermal compressibility. One may therefore expect that the ratio $\delta N/N$ becomes smaller as l^* becomes larger for constant T^* and n^*. This is also observed. There also seems to be some variation across the cell (approximately constant pressure, but changing temperature and density). This is consistent with Eq. (47). For $n^* = 0.1$, $\delta N/N$ is somewhat larger in the small volume elements than in the large, and a typical ratio is 0.2. From our data for the overall compression factor for the entire system, $Z = PV/NkT$, at $T^* = 2$ and three densities, we have estimated the isothermal compressibility of the system. Note that this is not the *local* value, but the thermodynamic property of the system. This gave $\delta N/N \approx (0.97/N)^{1/2}$ at $n^* = 0.1$, which is in excellent agreement with the data reported in Table III.

These results show that $\delta N/N$ depends weakly on the size of the control volume. Even for the largest control volume, $\delta N/N$ is an order of magnitude larger than Kreuzer's suggestion. The 512-particle system with $N_L = 32$ gave fluctuations that are consistent with the thermodynamic results, and the control volume must from this point of view be considered sufficiently large. Our largest control volume is about three times larger than that used by Tenenbaum *et al.*[5]

In order to further examine the effect of system size on the particle number fluctuation, the number of particles was increased from 512 to 4096, keeping $L_y/L_x = L_z/L_x = 0.5$. This increased l^* by a factor of 2 and the average particle number by a factor 8 compared to the numbers given in Table III. A system with 4096 particles is somewhat large for production runs at the workstations we used, both because the computation slows down (to 0.8 time steps per CPU second without optimization of the code for the larger system) and because the larger system requires longer time to reach a stationary state. A 1.5 million-time steps run was made, however, for $n^* = 0.1$. Fluctuations in the particle number were determined from the last 100,000 time steps. The results are given in parenthesis in Table III. The particle number fluctuation was reduced by a factor 3, which brings the control volume size in better accordance with Kreuzer's suggestion.[8] Again, this is in agreement with Eq. (47). The size of the control volume therefore does not seem to be critical in the cases we have studied. Our findings support the experience of Tenenbaum *et al.*[5] that $l^* \approx 1$ is reasonable, even if the lowest density we studied is low compared to a typical liquid density.

Our conclusion is that Kreuzer's suggestion is too conservative and that the reduced fluctuation in the particle number, and accordingly better statistics by increasing the system size, does not compensate for the drawbacks mentioned above by the size increase. The relatively large fluctuation in particle number is a warning that average quantities will require large

runs to achieve acceptable statistics, which indeed turned out to be the case in our runs. For practical reasons, we have therefore based most of our runs on the observation by Tenenbaum *et al.*[5] and used 512 particles with $N_L = 32$ for the production runs.

6.2. The Linear Regime and Validity of the Onsager Reciprocal Relations

Some of the calculations in this work can be seen as attempts to violate conditions of local equilibrium. The attempts were made because criteria for local equilibrium can only be tested by changing from local equilibrium to nonequilibrium conditions. The gradients in the algorithms we have used are limited by the condition that the temperature in the coldest layer must be positive and the mole fractions must be in the allowed range, [0, 1], in regions H and L. This leads to $\nabla T < 4T/L_x$ and $\nabla x_1 < 2/L_x$. These inequalities apply to the instantaneous values, and the averages will be more severely limited. Moreover, the system will enter into a solid–fluid two-phase state if the temperature in the cold region becomes too low.[19] As shown in Fig. 4, we have not been able to go beyond the linear regime. The results that are clearly in the linear regime provide satisfactory precision for the thermal conductivity and the diffusion coefficient. The data given in Table II show, however, that the cross-coefficients are not equally precise, because they represent relatively small contributions to the fluxes in stationary state.

The gradients are extremely large from an experimental point of view. For instance, our largest temperature gradient corresponds to a 4% change in T over one molecular diameter. The largest temperature gradient applied in this investigation is thus so large that it represents a situation which must be difficult, if not impossible, to realize in practice.

The results of Table II indicate that the Onsager reciprocal relations are valid in the middle region of the cell, despite the extreme temperature gradient applied. We must point out, however, that there is a discrepancy between our data for the thermal diffusion factor and those of Kincaid and Hafskjold[26] (using the fuzzy-wall algorithm) at $n^* = 0.1$ and 0.2. Ikeshoji[27] has simulated the same system with both algorithms in independently written codes, and confirmed that there is a discrepancy between the two methods. It is therefore unlikely that the discrepancy is due to a programming error. In the HEX algorithm, Ikeshoji[27] found that the equipartition principle is not satisfied in regions H and L at $n^* = 0.1$, probably because the heavier (slower) particles stay in these regions longer than the lighter particles do. The temperature profile near regions H and L is therefore steeper for the heavier than for the lighter component. This effect is

much less pronounced in region M, but it may have an impact on the value of the thermal diffusion factor and the analysis of the ORR. This problem does not arise for $n^* = 0.4$ or for the other transport coefficients, and therefore it will not affect most of the conclusions reached in this work. This methodological problem will be more thoroughly discussed in a forthcoming paper.

The discrepancy between the equilibrium and the nonequilibrium thermodynamic properties in the coldest layer shown in Fig. 8 made us suspect that the ORR might not be valid here. When the overall conditions of the cell were changed to the values of this layer, the ORR were verified also here, as shown in Table II. But uncertainties of the calculations are large, and a violation of the ORR may be masked.

MacGowan and Evans[6] and Paolini and Ciccotti[7] have reported results for coupled heat and mass transport in Lennard-Jones systems corresponding to an equimolar, liquid argon–krypton mixture. MacGowan and Evans found strong nonlinear flux–force relationships, but their *lowest* gradients were two orders of magnitude larger than our *highest* gradients. They found ORR to be valid, based on extrapolation of the flux–force relationships in the linear regime to zero forces. Paolini and Ciccotti also reported data for L_{1q} and L_{q1} in the linear regime, close to where MacGowan and Evans found onset of nonlinearity. They also verified the ORR. In both reports, the uncertainties were comparable to ours (8% in the ratio L_{q1}/L_{1q} at $n^* \approx 0.7$, whereas we have 6% at $n^* = 0.4$). The different algorithms are complementary in that the MacGowan–Evans algorithm is better suited to explore the nonlinear regime, whereas our algorithm seems better (i.e., more precise estimates) for the linear regime.

Our results for the Onsager reciprocal relationships (Table II) do not give any new information compared to the findings of MacGowan and Evans, and Paolini and Ciccotti. The question of the validity of the ORR outside the linear regime is still not solved. At this point we may thus still speculate that ORR are valid beyond local equilibrium, even if originally proven for local equilibrium.

6.3. Thermodynamic State Functions in a Stationary State Transport Process

Given that the gradients of the system are severe, it is remarkable to see that the criterion of local equilibrium formulated by Tenenbaum *et al.*[5] is fulfilled (see Fig. 8). It appears that the only discrepancy generated between the system properties and the corresponding value given by an equilibrium state function is obtained for the pressure in the coldest layer of the cell. The properties of the coldest layer discussed in Section 6.2 show

that the effect is a boundary effect rather than a consequence of the conditions. Tenenbaum *et al.* also found that the criterion was satisfied under similar conditions, except in their hottest layer. They ascribed this to a boundary effect.

The validity of Tenenbaum's criterion has an important consequence: We may use the basic equations of thermodynamics to describe stationary state systems with transport even under experimentally extreme conditions.

This conclusion is further strengthened by the results for the Boltzmann H-function of the system. The results for the H-function of the lowest densities of Table II, having the largest uncertainties in the Onsager reciprocal relations, show agreement within 3% with the results of an equilibrium Maxwell–Boltzmann distribution, as shown in Fig. 9. Being an integral of the velocity distribution, this agreement does not prove that the velocity distributions in the control volume is identical to a Maxwell–Boltzmann distribution. The sensitivity of the H-function to variations in the velocity distribution is therefore interesting.

The H-function relaxation to stationary state distribution starting from a rectangular distribution of velocities was quite rapid, within some 4000 time steps at the most (Fig. 10). The relaxation of the heavy particles (component 1) is faster in the cold region than in the hot region (data not shown). This can be understood from the fact that the intermolecular energy transfer by interactions of this component contributes more at the cold side compared to the hot side.[20] At intermediate densities ($n^* = 0.4$), component 1 exchanges more energy with its neighbors than component 2 does in the cold region, whereas the opposite is true in the hot region.

Our results confirm the discussion by Haile[11] in that the H-function is capable of measuring a deviation from a Maxwell–Boltzmann distribution. The relaxation time of the H-function is short compared to the time used to compute averages of thermodynamic functions in every volume element of the system, but long compared to a time step. The data show that the time-averaged H-function is not very sensitive to *external constraints* (i.e., gradients) imposed on the volume element, and it is consistent with the other criteria discussed here.

In a recent paper on NEMD simulations of an isotope mixture at higher densities, we speculated that the system was not in local equilibrium in the regions of the heat source and sink, possibly because it was unable to dissipate the exchanged energy at a sufficient rate.[19, 20] The relaxation rate of H confirms this mechanism.

The instantaneous H-function is clearly sensitive to the velocity distribution, as shown in Fig. 10. The reason why this does not show up in the time average can be understood from the following argument: When energy is pumped into (out of) the system in region H (L) at *every* time

step, one might expect the velocity to become non-Maxwellian. If, however, β is small compared to $(1+\alpha)v_i$ [cf. Eq. (24)], the velocity distribution will preserve its Maxwellian form even if the system is excited.

6.4. Flux–Force Relationships from Local Equilibrium Criteria

The fluctuation criterion of Kreuzer, Eq. (3a), is not very specific. The value of $\delta T/T$ in this investigation is everywhere higher than 0.01 (i.e., 1% deviation in the computed averages), but not by very much (see Table III and Fig. 7). The highest value (0.04) is obtained for the *lowest* density. The temperature fluctuation is related to the heat capacity at constant volume c_V by

$$\frac{\delta T}{T} = \left(\frac{k}{Nc_V}\right)^{1/2} \tag{48}$$

We estimated the heat capacity from five equilibrium runs at $n^* = 0.1$ around $T^* = 2.0$, and numerical differentiation. This gave $\delta T/T \approx (0.6/N)^{1/2}$. The fluctuations reported in Table III are much smaller than expected from the heat capacity of the equilibrium system.

We can therefore conclude that $\delta T/T \approx 0.03$ can be used as a more specific fluctuation criterion at $n^* = 0.1$ and $T^* = 2.0$. This is fulfilled everywhere in the cell with $N_L = 32$. We expect that this conclusion is equally valid at $n^* = 0.2$ and 0.4.

The variation in $\delta T/T$ across the cell is interesting. The fluctuation in T in any control volume has, as shown in Fig. 7, about the same magnitude as the difference in average temperature between two adjacent layers, except in the coldest layer. This property may be important for the validity of linear flux–force relations because the energy level of the next step in the transport process must be within reach by excitation of the molecules involved. This gives a certain continuity in the transfer of energy, and is therefore a physical concept behind linear transport equations. The exception to this in the low-temperature layer is another indication of lack of local equilibrium in this region.

The criteria for local equilibrium represented by Eqs. (7) extend Kreuzer's criterion ($l\,|\nabla T|/T \leqslant \delta T/T \ll 1$). The condition $\mathbf{J}_q/\mathbf{J}_q^0 < 0.3$ is implied, consistent with linear flux–force relations. In our case, $l\,|\nabla T|/2T \approx 0.02$ at $n^* = 0.1$ with $N_L = 32$, which agrees well with the temperature fluctuation, and linearization seems well justified. If the analog of the overpotential theory is right, this would correspond to $\mathbf{J}_q/\mathbf{J}_q^0 \approx 0.02$. The directly computed value is 0.2, however. Similarly, the largest gradient in chemical potential (composition) gives $l\,|\nabla_T(\mu_1 - \mu_2)|/2kT \approx 0.2$, which

still justifies linearization. This would correspond to $\mathbf{J}_1/\mathbf{J}_1^0 \approx 0.2$, whereas the computed value is 8. Both the heat flux and the mass flux are underestimated by at least an order of magnitude.

These results taken *separately* both indicate that we are outside the range of linear flux–force relationships, while the results discussed in Section 6.2 clearly show that this is not the case. Possible explanations are that its theoretical foundation is wrong or that Eq. (7) does not apply to our case. The foundation is semiempirical and limited to a transport mechanism for a single process with a well-defined energy barrier. This is not the case for our fluid system. MD simulations have shown that even diffusion in *solids* cannot be explained in terms of this mechanism.[28] Furthermore, we consider here *coupled* transport processes. The total system then transports heat more effectively and with less entropy production, which may be one explanation for an extended range of linearity. This can be seen from

$$\sigma = \left(L_{qq} - \frac{L_{q1}L_{1q}}{L_{11}}\right)\left(\frac{\nabla T}{T^2}\right)^2 - \left(\frac{L_{q1} - L_{1q}}{L_{11}}\right)\mathbf{J}_1 \cdot \frac{\nabla T}{T^2} + \frac{J_1^2}{L_{11}} \tag{49}$$

which is derived from Eq. (1) by using Eq. (2b) to eliminate the force $\nabla_T(\mu_1 - \mu_2)/T$. The second term at the right-hand side of Eq. (49) vanishes due to the ORR. At stationary state with $\mathbf{J}_1 = 0$, the third term vanishes. The entropy production is smaller for the inhomogeneous mixture than for the homogeneous mixture with the same $\nabla T/T$, because L_{qq} is reduced to $L_{qq} - L_{q1}L_{1q}/L_{11}$. The reduction in σ and $\mathbf{J}_q$ is small (6%), however, which is not consistent with an order-of-magnitude error in $\mathbf{J}_q/\mathbf{J}_q^0$.

6.5. General Comments

One practical result of this work is that the equilibrium exchange flux (or the unidirectional flux) can be equated to the fluctuation in the stationary state flux value.

One might argue that the present MD simulations cannot violate microscopic reversibility and the ORR because of the inherent reversibility in Newton's equations of motion. In a NEMD algorithm, it is the *boundary conditions* that introduce the irreversibility, and the system as a whole is non-Newtonian. A particle sufficiently apart from the boundaries will behave Newtonian-like and obey microscopic reversibility. By "sufficiently apart" we mean that its memory of the boundaries must have been lost during the diffusion, and the intermolecular energy transfer contribution to the heat flux must be small. A thermal shock wave, for instance, would not satisfy this.

The present analysis was performed on the problem of coupled transport of heat and one independent mass component. There are good reasons to believe that the discussion of this system applies to other cases, as the criteria used are of general nature; some are partly inspired from the theory of overpotentials. We shall proceed with this work to investigate the coupled transport of charge and mass from the same perspective, using parts of the scheme developed in this article.

7. CONCLUSIONS

A binary mixture of isotopes with mass ratio $m_1/m_2 = 10.0$ has been studied in a system which transports heat and mass. Within the context of the accuracy of the present NEMD simulations, the following conclusions can be drawn from the study:

- Kreuzer's recommendation for the control volume size, $\delta N/N \ll 10^{-2}$, is too conservative for the cases we have studied. Our data support the findings of Tenenbaum *et al.* that the thickness of the control volume can be of the order one average intermolecular distance.

- Under conditions of a high temperature gradient, equilibrium thermodynamic properties can be calculated for all local volume elements of the cell, except near the boundaries. This implies that the basic equations of thermodynamics can be used to describe systems under severe gradients in the stationary state.

- Away from the boundaries, the Boltzmann H-function of the system is consistent with the Maxwell–Boltzmann distribution within 1%. The relaxation of the H-function, typically within 4000 time steps, lends further support to the result that the local volume elements in the stationary state system can be described by equilibrium thermodynamics.

- The temperature fluctuation was found to be $\delta T/T \approx 0.03$. This value is in agreement with the criterion proposed by Kreuzer ($\delta T/T \ll 1$).

- A criterion inspired by the overvoltage theory has been examined. The ratio of a net flux and the equilibrium exchange flux is here linked to a condition for linear flux–force relationships. This criterion indicates that we are in the range of linear flux–force relationships in the present investigation, which is consistent with our data. It gives, however, estimates for the fluxes that are off by at least one order of magnitude. The effect of coupling between heat and mass transport gives an extension of the linear regime of the transport process.

- Within uncertainties given by the calculations, the Onsager reciprocal relations are valid for the system.

• The NEMD analysis has proved a useful tool in obtaining answers to questions regarding criteria on local equilibrium. Some of the computed quantities, i.e., the equilibrium exchange flux, cannot be obtained otherwise, e.g., from experiments. The application of NEMD may therefore contribute to making phenomenological descriptions less dependent on experiments.

ACKNOWLEDGMENTS

We gratefully acknowledge John M. Kincaid for discussions during the development of the MEX algorithm and for checking some of our computer code and data, and Tamio Ikeshoji for repeating some of our runs with his independent code.

REFERENCES

1. L. Onsager, Reciprocal relations in irreversible processes. I, *Phys. Rev.* **37**:405–426 (1931).
2. R. M. Velasco and L. S. Garcia-Colin, The kinetic foundations of non-local non-equilibrium thermodynamics, *J. Non-Equilib. Thermodyn.* **18** (1993), in press.
3. K. Olah, Thermokinetics (an introduction), *Periodica Polytechnica Chem. Eng.* **31**:19–27 (1987).
4. K. Olah, Thermostatics, thermodynamics, and thermokinetics, *Acta. Chim. Hung.* **125**:117–130 (1988).
5. A. Tenenbaum, G. Ciccotti, and R. Gallico, Stationary nonequilibrium states by molecular dynamics. Fourier's law, *Phys. Rev. A* **25**:2778–2787 (1982).
6. D. MacGowan and D. J. Evans, Heat and matter transport in binary liquid mixtures. *Phys. Rev. A* **34**:2133–2142 (1986); see also D. J. Evans and D. MacGowan, Addendum to "Heat and matter transport in binary liquid mixtures," *Phys. Rev. A* **36**:948 (1987).
7. G. V. Paolini and G. Ciccotti, Cross thermotransport in liquid mixtures by non-equilibrium molecular dynamics, *Phys. Rev. A* **35**:5156–5166 (1987).
8. H. J. Kreuzer, *Nonequilibrium Thermodynamics and its Statistical Foundations* (Clarendon, Oxford, 1981).
9. J. Meixner, Zur Thermodynamik der irreversiblen Prozesse, *Z. Phys. Chem. B* **53**:235–263 (1941).
10. J. Meixner, Zur Thermodynamik der irreversiblen Prozesse in Gasen mit chemisch reagierenden, dissozierenden und anregbaren Komponenten, *Ann. Phys.* (Leipzig) **43**:244–270 (1943).
11. J. M. Haile, *Molecular Dynamics Simulations. Elementary Methods* (Wiley, New York, 1992).
12. J. Orban and A. Bellemans, Velocity-inversion and irreversibility in a dilute gas of hard disks, *Phys. Lett.* **24A**:620–621 (1967).
13. H. Eyring and E. Eyring, *Modern Chemical Kinetics* (Rheinhold, New York, 1963).
14. J. Goodisman, *Electrochemistry: Theoretical Foundations* (Wiley-Interscience, New York, 1987).
15. K. S. Førland, T. Førland, and S. K. Ratkje, *Irreversible Thermodynamics. Theory and Applications* (Wiley, Chichester, England, 1988).

16. T. L. Hill, On the one-dimensional steady-state Ising problem, *J. Chem. Phys.* **76**:1122–1127 (1982).
17. S. R. Caplan and A. Essig, *Bioenergetics and Linear Nonequilibrium Thermodynamics. The Steady State* (Harvard University Press, Cambridge, Massachusetts, 1983).
18. K. D. Garlid, A. D. Beavis, and S. K. Ratkje, On the nature of ion leaks in energy-transducing membranes, *Biochim. Biophys. Acta* **976**:109–120 (1989).
19. T. Ikeshoji and B. Hafskjold, Nonequilibrium molecular dynamics calculation of heat conduction in liquid and through liquid–gas interface, *Mol. Phys.* (1993), in press.
20. B. Hafskjold, T. Ikeshoji, and S. K. Ratkje, On the molecular mechanism of thermal diffusion in liquids, *Mol. Phys.* (1993), in press.
21. R. Haase, *Thermodynamics of Irreversible Processes* (Addison-Wesley, Reading, Massachusetts, 1969).
22. D. J. Evans and G. P. Morriss, *Statistical Mechanics of Nonequilibrium Liquids* (Academic Press, London, 1990).
23. P. Sindzingre, C. Massobrio, and G. Ciccotti, Calculation of partial enthalpies of an argon–krypton mixture by *NPT* molecular dynamics, *Chem. Phys.* **129**:213–224 (1989).
24. B. L. Holian and D. J. Evans, Shear viscosities away from the melting line: A comparison of equilibrium and nonequilibrium molecular dynamics, *J. Chem. Phys.* **78**:5147 (1983).
25. J. M. Kincaid, X. Li, and B. Hafskjold, Nonequilibrium molecular dynamics calculation of the thermal diffusion factor, *Fluid Phase Equilib.* **76**:113 (1992).
26. J. M. Kincaid and B. Hafskjold, Thermal diffusion factors for the Lennard-Jones/spline system, *Mol. Phys.*, submitted.
27. T. Ikeshoji, private communication.
28. X. Li, Ion transport in solid electrolytes studied by molecular dynamics simulations, Ph.D. Thesis no. 57, University of Trondheim, The Norwegian Institute of Technology.